

# Enhancing pDNA Delivery with Hydroquinine Polymers by Modulating Structure and Composition

Punarbassu Roy, Nicholas W. Kreofsky, Mary E. Brown, Craig Van Bruggen, and Theresa M. Reineke\*

Cite This: *JACS Au* 2023, 3, 1876–1889

Read Online

ACCESS |

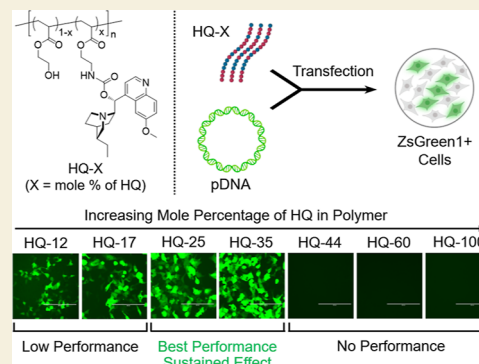
Metrics & More

Article Recommendations

Supporting Information

**ABSTRACT:** Quinine is a promising natural product building block for polymer-based nucleic acid delivery vehicles as its structure enables DNA binding through both intercalation and electrostatic interactions. However, studies exploring the potential of quinine-based polymers for nucleic acid delivery applications (transfection) are limited. In this work, we used a hydroquinine-functionalized monomer, HQ, with 2-hydroxyethyl acrylate to create a family of seven polymers (HQ-X, X = mole percentage of HQ), with mole percentages of HQ ranging from 12 to 100%. We developed a flow cytometer-based assay for studying the polymer–pDNA complexes (polyplex particles) directly and demonstrate that polymer composition and monomer structure influence polyplex characteristics such as the pDNA loading and the extent of adsorption of serum proteins on polyplex particles. Biological delivery experiments revealed that maximum transgene expression, outperforming commercial controls, was achieved with HQ-25 and HQ-35 as these two variants sustained gene expression over 96 h. HQ-44, HQ-60, and HQ-100 were not successful in inducing transgene expression, despite being able to deliver pDNA into the cells, highlighting that the release of pDNA is likely the bottleneck in transfection for polymers with higher HQ content. Using confocal imaging, we quantified the extent of colocalization between pDNA and lysosomes, proving the remarkable endosomal escape capabilities of the HQ-X polymers. Overall, this study demonstrates the advantages of HQ-X polymers as well as provides guiding principles for improving the monomer structure and polymer composition, supporting the development of the next generation of polymer-based nucleic acid delivery vehicles harnessing the power of natural products.

**KEYWORDS:** gene delivery, quinine, transfection, pDNA delivery, cinchona alkaloids, nonviral gene therapy, controlled polymerization, natural product polymer



## INTRODUCTION

The field of gene therapy has undergone exponential growth in the last decade.<sup>1–4</sup> Out of the 24 gene therapy products that are currently available for patients, 18 of them have been approved since 2017.<sup>5,6</sup> As of the fourth quarter of 2022, more than 2000 gene therapy products are in the discovery pipeline with the potential to treat diseases that currently have no medical interventions.<sup>5</sup> One of the crucial steps for success is the functional delivery of therapeutic nucleic acid into the cells. Most clinical trials have been developed around the use of recombinantly engineered viruses as the delivery vehicle or vector.<sup>7,8</sup> Despite their efficiency, viral delivery of genetic material is limited by factors such as small cargo capacity, exorbitant cost of manufacturing, poor scalability, and risk of immunogenicity.<sup>9–12</sup> The power of nonviral delivery methods has been exemplified by the success of the COVID-19 vaccines, which are packaged in lipid-based vehicles.<sup>13</sup> Polymer-based gene delivery vehicles have emerged as a promising alternative due to their facile scalability, ease of manufacturing, thermal stability, and wide chemical space for optimizing their design optimized to application.<sup>14–16</sup>

Cationic polymers, which typically host amine groups, have been shown to bind with negatively charged nucleic acids and package them into nanoparticle complexes known as polyplexes. Many studies have contributed to furthering our understanding of the role of structural parameters such as identity of cation/amine groups, molar mass of the polymers, charge density, and architecture on polymer-mediated gene delivery, i.e., transfection.<sup>14–18</sup> However, most of them have utilized polymers synthesized from commercially available monomers, which facilitate binding between the polymer and nucleic acid only via electrostatic interactions. The use of natural product-based monomers with known pharmacological properties that promote polymer–nucleic acid binding via alternative modes (non-electrostatic interactions) remains

Received: March 17, 2023

Revised: May 26, 2023

Accepted: June 12, 2023

Published: June 28, 2023



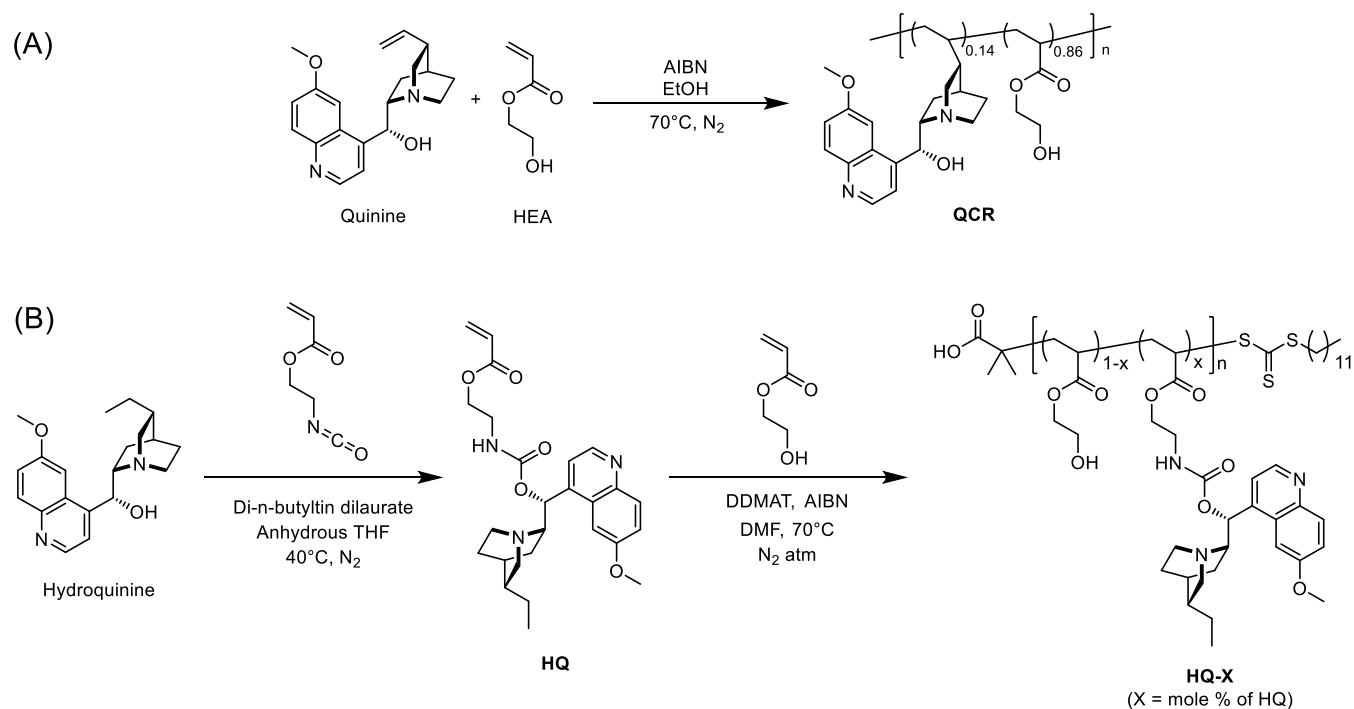


**Figure 1.** (A) Synthesis scheme and chemical structure of the QCR.<sup>31</sup> (B) Synthesis scheme for the HQ monomer and copolymerization of HQ with HEA using the controlled polymerization method of RAFT.

relatively underexplored, limiting the chemical diversity and tunability of the polymers to their application. A key known example is the alkaloid compound and antimalarial drug, chloroquine, which has long been used to facilitate endosomal escape of nonviral delivery agents.<sup>19,20</sup> Chloroquine is a lysosomotropic agent, i.e., it gets accumulated in the vesicles of the endocytosis pathway where the polyplexes also get localized. At elevated concentrations inside the endosomal vesicles, chloroquine prevents degradation of the delivered nucleic acid by buffering the acidic endosomal pH. Additionally, chloroquine facilitates unpacking of the nucleic acid payload from the polyplexes as it competitively interacts with the nucleobases and the negatively charged phosphate groups through electrostatic interaction.<sup>21,22</sup> Taking advantage of these properties of chloroquine, Oupický and co-workers have developed and studied chloroquine-containing polymers for efficient delivery of anti-miRNA.<sup>23</sup> Their results established the incorporation of chloroquine in the polymers as an advantageous strategy to improve the gene delivery efficiency of polymer-based vehicles.

Another similar alkaloid and antimalarial compound, quinine,<sup>24–26</sup> has been shown to bind with DNA through electrostatic and intercalation interactions.<sup>27,28</sup> There has been some success in synthesizing quinine-based copolymers using free radical and step growth polymerization but there are no reports of controlled polymerization of quinine.<sup>29,30</sup> Our previous work has demonstrated the synthesis of several quinine-based copolymers via direct free-radical copolymerization of this natural product with monomers such as 2-hydroxyethyl acrylate (HEA), *N*-hydroxyethyl acrylamide, methyl acrylate, and *N*-isopropylacrylamide. However, we were only able to incorporate quinine up to 17%.<sup>31</sup> From that family of copolymers, the copolymer of quinine and HEA (QCR) (Figure 1A) showed remarkable efficiency in delivering plasmid DNA (pDNA) to a wide range of cells with

transfection efficiency comparable to a commercial standard, Lipofectamine 2000. Furthermore, Raman spectroscopic studies on the vibrational modes of quinine provided insights into protein-mediated polyplex unpacking in the cellular environment, without the use of any additional labeling.

In this work, we sought to understand the role of quinine composition on the pDNA delivery performance of polymer vehicles along with cellular mechanisms, to elucidate and optimize design principles for improving quinine-based polymers from that of our previous model (QCR) created via free-radical polymerization (FRP). We hypothesized that modulating quinine composition within the copolymers will significantly impact polymer–pDNA interactions, delivery efficiency, and resultant transgene expression. To study this hypothesis, we synthesized a hydroquinine-functionalized monomer, HQ, that unlike quinine, was compatible with the controlled polymerization method of reversible addition–fragmentation chain transfer (RAFT). Using HEA as the comonomer, a family of polymers was synthesized with the mole percentage of HQ, ranging from 12 to 100% (HQ-X, X = mole % of HQ). Furthermore, we developed a flow cytometer-based assay to probe the influence of the polymer composition on the amount of pDNA loaded in the polyplex particles, assess the relative adsorption of serum proteins on these particles, and the extent of cargo unpacking that is facilitated by the serum proteins. We find that the polymer's ability to bind with pDNA increases monotonically with increasing mole percentage of HQ in the polymer chain, but maximum transfection efficiency *in vitro* is obtained with 25–35% HQ content owing to the optimum balance between polymer–pDNA binding and release of pDNA after cellular internalization. As HQ is structurally similar to chloroquine, well known for its ability to rupture endosomal vesicles via the proton sponge mechanism, we performed confocal imaging to determine if HQ-X polymers are also efficient in perturbing the

**Table 1. Molecular Characteristics of the HQ-X Polymers**

Code	Method	% HQ in chain	$M_w$ (kDa)	$M_n$ (kDa)	$\bar{D}$	$pK_a$	$n_{\text{Hill}}$
HQ-12	RAFT	12	19	16	1.24	7.0	0.9
HQ-17	RAFT	17	22	17	1.29	6.6	1.3
HQ-25	RAFT	25	24	19	1.28	6.6	1.5
HQ-35	RAFT	35	25	19	1.28	6.3	1.7
HQ-44	RAFT	44	35	25	1.39	6.3	1.7
HQ-60	RAFT	60	21	16	1.33	6.2	1.7
HQ-100	FRP	100	39	20	1.91	6.2	1.6

endosomes allowing the pDNA payload to escape into cell cytoplasm. Our quantitative analysis indicates a low correlation between the spatial distribution of pDNA payload and lysosomes inside the cells, suggesting that HQ-X polymers are indeed efficient in facilitating the release of the pDNA payload from the endosomal vesicles. Compared to HQ ( $pK_a = 8.3$ ), the HQ-X polymers have lower  $pK_a$  (6–7) and consequently have a larger reserve of unprotonated amines that act like proton sponges contributing to the endosomal escape by HQ-X polyplexes. We also highlight the advantage of the highest-performing polymers in this family, HQ-25 and HQ-35, in sustaining the effects of transfection over a longer period of time outperforming the commercially available transfection agents. Overall, this study showcases the utility of using HQ to access a wide range of statistical copolymers that bind to pDNA via intercalation and electrostatics and that intermediate levels of HQ incorporation provide the best results for transfection. To the best of our knowledge, this is the first demonstration of controlled polymerization of a hydroquinine-functionalized monomer, and this approach will enable controlled polymerization of similar alkaloids. Moreover, this work contributes to the fundamental design principles applied for optimizing the nucleic acid delivery performance of natural product-based polycations.

## RESULTS AND DISCUSSION

### Synthesis

Despite having a reactive alkene functionality, facile and controlled polymerization of quinine has remained elusive. The difficulty with polymerizing quinine via radical polymerization potentially lies in the degradative chain transfer of the propagating secondary radical, generated at the alkene, to one of the three tertiary carbon centers in the quinuclidine fragment of quinine.<sup>32</sup> This leads to the formation of a stable tertiary carbon radical and termination of the propagating polymer chain. Instead of using quinine directly, derivatives of quinine have been used to synthesize various polymers that were otherwise inaccessible with free-radical copolymerization of quinine.<sup>33–36</sup> In this current work, we synthesized an acrylate analogue of hydroquinine, HQ, by coupling hydroquinine with 2-isocyanatoethyl acrylate due to the higher propensity of acrylates toward polymerization than simple alkenes (Figures 1B and S1–S3).<sup>37</sup> Hydroquinine was chosen over quinine, as the precursor, to have only one polymerizable alkene on the final monomer, minimizing undesired chain transfer or cross-linking events during polymerization.<sup>32</sup> To our advantage, unlike quinine, HQ was found to be compatible with RAFT copolymerization. A series of copolymers of HQ and HEA, with mole percentage of HQ in the polymer chain varying from 12 to 60%, were synthesized via RAFT copolymerization (Figures 1B and S4–S6, and Table 1 and

Table S1). Furthermore, HQ was amenable to free-radical homopolymerization, which has not been possible with quinine (Tables 1 and S1, Figure S4). This family of polymers consisted of the six copolymers synthesized via RAFT and the homopolymer of HQ synthesized via FRP and are collectively referred to as HQ-X polymers, where X represents the mole percentage of HQ in the polymer (Table 1).

### Determining the Protonation State

Electrostatic interactions between the polymer and pDNA, as well as the endosomal escape of polyplexes depend on the protonation state of the polymer, and these properties ultimately affect the efficiency of polymer-mediated transfection.<sup>14</sup> In quinine, there are two nitrogen centers able to be protonated—one at the quinuclidine group ( $pK_a = 8.5$ ) and the other at the quinoline ring ( $pK_a = 4.1$ ).<sup>38</sup> Consistent with our previous work, we have studied the protonation state of the quinuclidine nitrogen center of the HQ-X polymers since that is the only relevant protonable nitrogen at physiological pH. To understand how polymer composition influences the protonation state of the polymers in aqueous solution, the  $pK_a$  and the Hill coefficient ( $n_{\text{Hill}}$ ) for the monomer as well as the polymers were determined using potentiometric titration. Compared to HQ ( $pK_a = 8.3$ ), the polymers had lower  $pK_a$  ( $\leq 7.0$ ) (Table 1, Figure S7). Such depression of  $pK_a$  from monomer to polymer, due to electrostatic repulsion among amine groups in proximity, aligns with previous reports.<sup>39,40</sup> We also observe that the decrease in  $pK_a$  is correlated with the polymer composition, i.e.,  $pK_a$  of the polymers decreases as the mole percentage of HQ in the polymer chain increases, likely due to increased interactions among the HQ repeat units.<sup>39,40</sup> The low  $pK_a$  of HQ-X polymers suggests that only a small fraction of amines is present in the protonated state, at the physiological pH of 7.4, available for electrostatic interactions with pDNA. However, we speculated that the large reserves of unprotonated amines can act like a proton sponge, promoting endosomal escape and aiding in gene delivery to the cell nucleus.<sup>41–43</sup> Furthermore, we also hypothesized that higher amount of HQ will increase polymer–pDNA binding through enhanced intercalation. Other than the  $pK_a$ , the significance of cooperativity of protonation in the polymers, in the context of gene delivery, has been suggested in recently published work.<sup>39,44</sup> The Hill coefficient ( $n_{\text{Hill}}$ ) is a measure of cooperativity in the protonation–deprotonation process, and polymer hydrophobicity has been shown to influence this parameter.<sup>39</sup> A value of  $n_{\text{Hill}} \sim 1$  implies that the amine groups in the polymer undergo protonation (or deprotonation) independent of other amine groups in their proximity. However,  $n_{\text{Hill}} > 1$  suggests positive cooperativity in protonation (or deprotonation), which means protonation (or deprotonation) of one amine group facilitates protonation (or deprotonation) of the surrounding amine groups. Similar to  $pK_a$ , a correlation is observed between the polymer

composition and  $n_{\text{Hill}}$ —the value of  $n_{\text{Hill}}$  increases with the increase in the mole percentage of HQ (Table 1, Figure S7). As HQ is quite hydrophobic ( $\text{clog}P = 4.21$ ),<sup>45</sup> the aqueous solubility of the polymers decreases with the increase in the mole percentage of HQ. Quinine is also known to interact with itself at higher concentrations, and the same can be expected for HQ when it is incorporated into the polymer chain.<sup>46</sup> The hydrophobic nature of HQ and the self-interactions among HQ repeat units explain the increase in  $n_{\text{Hill}}$  with the increase in the percentage of HQ in the polymer chain. It has been suggested in the previous reports that polymers with higher  $n_{\text{Hill}}$  are capable of releasing their payload rapidly inside the cell cytosol in comparison to the polymers possessing lower  $n_{\text{Hill}}$  and therefore have higher gene delivery efficiency.<sup>17,39</sup> Based on those previous findings, we anticipated the efficiency of delivering pDNA into the cell nucleus to gradually increase with the increase in the percentage of HQ in the polymer chain. Overall, the unconventionally low  $\text{p}K_{\text{a}}$  values and cooperativity of the protonation/deprotonation process ( $n_{\text{Hill}} > 1$ ) add to the novelty of HQ-X polymers, and in the later sections, we discuss what influence these parameters have on the gene delivery efficiency.

### Probing Polymer–pDNA Binding

The ability of these polymers to bind with and compact pDNA into polyplexes was evaluated using a dye exclusion assay, at different  $N/P$  ratios, where  $N$  stands for the number of moles of quinuclidine nitrogen atoms and  $P$  stands for the number of moles of phosphate groups from pDNA in the solution. In this assay, pDNA was first mixed with PicoGreen, a molecule that is fluorescent when intercalated in the pDNA ( $\lambda_{\text{ex}} = 485 \text{ nm}$ , and  $\lambda_{\text{em}} = 528 \text{ nm}$ ). Subsequently, the polymer solutions were added to the pDNA-PicoGreen mixture at different  $N/P$  ratios to allow the formation of polyplexes. The decrease in the fluorescence intensity, resulting from the exclusion of PicoGreen from pDNA due to competitive binding and pDNA compaction, was measured (Figure 2A). For all the polymers, increasing the  $N/P$  ratio resulted in a decrease in fluorescence intensity, indicating stronger binding between polymers and pDNA at higher  $N/P$ . More importantly, at all  $N/P$  ratios, polymer–pDNA binding increases monotonically with the increase in mole percentage of HQ. Interestingly, QCR, with only 14% quinine incorporation, shows stronger binding to pDNA compared to HQ-12 and HQ-17 despite the comparable molar composition of the polymers. In fact, QCR shows stronger binding than HQ-25 (Figure 2B). This difference in binding strength can be attributed to the differences in the monomer structure and orientation of the side chain in polymers. Unlike QCR, HQ-X polymers do not possess the hydroxyl group that can participate in hydrogen bonding with the pDNA (Figure 1). Our previous work using molecular dynamic simulations has shown that the hydroxyl group in quinine can interact with nucleobases in DNA through hydrogen bonding interactions.<sup>27</sup> Therefore, we believe that the lack of the hydroxyl group on the HQ repeat unit, in contrast to quinine, results in relatively weaker binding with pDNA compared to QCR, at comparable molar composition. These results demonstrate that other than electrostatic and intercalation interactions, hydrogen bonding plays an important role in dictating the characteristics of polymer–pDNA binding.

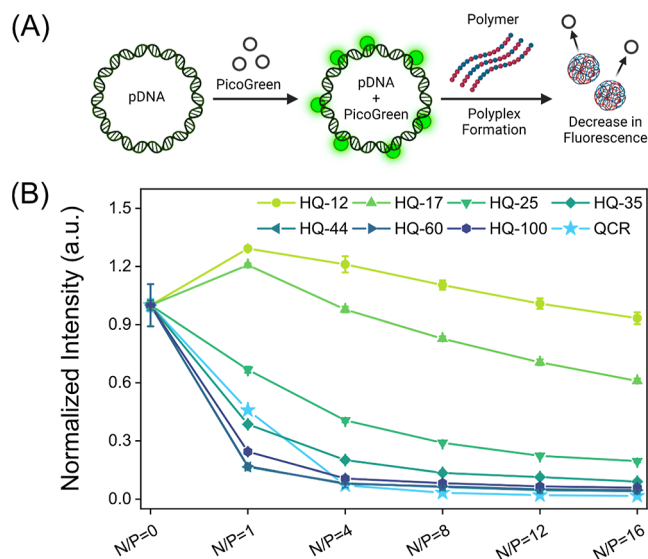


**Figure 2.** (A) General scheme for the dye exclusion assay. Intercalation of PicoGreen in pDNA results in bright green fluorescence. Binding of polymer with pDNA and the subsequent compaction leads to exclusion of PicoGreen from the pDNA resulting in decrease in fluorescence intensity. (B) Normalized fluorescence intensities from the dye exclusion assay. For all  $N/P$  ratios, higher mole percentage of HQ in polymer leads to stronger binding and compaction of pDNA, as indicated by the gradual decrease in the fluorescence intensity.

### Aggregation Behavior of Polyplexes

Polyplex size has a significant impact on the gene delivery efficiency as cell membrane adhesion, cellular internalization, and intracellular trafficking of polyplexes are size dependent.<sup>47</sup> In our previous work, we demonstrated that QCR complexes with pDNA to initially form polyplexes that are 80 to 200 nm in hydrodynamic diameter ( $d_h$ ). Upon dilution with serum-free cell culture media, polyplexes of QCR form large aggregates ( $d_h > 1000 \text{ nm}$ ), owing to the hydrophobicity of quinine in physiological pH ( $\sim 7.4$ ). The large size of the polyplexes was found to be advantageous for in vitro transfection as the polyplex particles settled on the cells faster. Since HQ is hydrophobic as well ( $\text{clog}P = 4.21$ ),<sup>45</sup> we anticipated that polyplexes formed with HQ-X will also aggregate at physiological pH, and increasing the mole percentage of HQ in the polymer will result in an increase in the polyplex size. Using dynamic light scattering (DLS), we observed that all the HQ-X polymers form polyplex particles by binding with pDNA, and the particle sizes ( $d_h$ ) range between 50 and 100 nm. Dilution of the polyplex solution with serum-free media (FluoroBrite DMEM) causes these polyplex particles to aggregate over time and grow up to 1000 nm or larger, in diameter, within 30 min (Figure S8, Table S2). In general, a higher mole percentage of HQ in the polymer leads to faster aggregation and larger particles. At mole percentages of HQ higher than 35%, the polyplexes show a high propensity for aggregation pushing them beyond the scope of DLS measurements ( $d_h > 1500 \text{ nm}$ ). Since internalization of the polyplex particles is a size-dependent phenomenon, we anticipated low transfection efficiency from the formulations that resulted in the largest aggregates potentially due to poor internalization. However, the results from cellular uptake experiments discussed later provide evidence that even the polymers

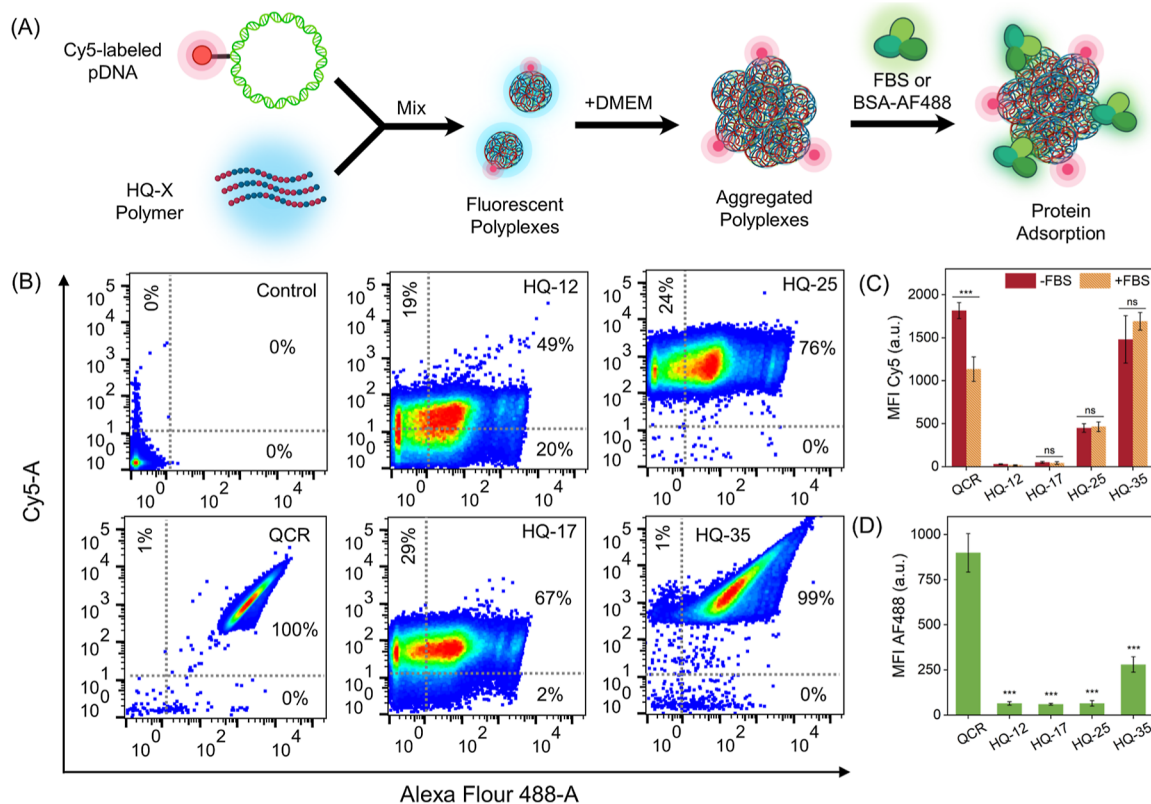


**Figure 3.** Flow cytometric analysis of aggregated polyplex particles. (A) Scheme for forming fluorescently labeled aggregated polyplexes using HQ-X polymers and Cy5-labeled pDNA. The influence of the polymer composition on protein adsorption on the aggregated polyplexes was studied by incubating the aggregated polyplexes with either FBS or Alexa Fluor 488-labeled bovine serum albumin (BSA-AF488). (B) Flow cytometry scatter plots of the aggregated polyplexes formed using different polymers. Cy5 intensity is on the Y-axis, and Alexa Fluor 488 intensity is on the X-axis. (C) Geometric mean fluorescence intensity of Cy5 from the aggregated polyplexes before and after incubation with FBS. Aggregated polyplexes of QCR have higher pDNA loading compared to HQ-12, HQ-17, and even HQ-25. While HQ-X polymers have lower loading capacity for pDNA, their polyplexes were found to be more resistant to protein-mediated payload unpacking compared to QCR. Statistical significance was evaluated using two-way ANOVA followed by Sidák's multiple comparisons test ( $***p \leq 0.001$ ). (D) Geometric mean fluorescence intensity of Alexa Fluor 488 from the aggregated polyplexes. HQ-X polymers show significantly low protein adsorption compared to QCR. Statistical significance was evaluated using one-way ANOVA followed by Dunnett's multiple comparisons test ( $***p \leq 0.001$ ).

producing the largest aggregates can deliver pDNA inside the cells.<sup>47</sup>

### Flow Cytometry on Polyplexes

The characteristics of the aggregated polyplex particles formed with HQ-12, HQ-17, HQ-25, and HQ-35 as well as QCR were studied in more detail using flow cytometry since their sizes ranged above the lower limit of detection (diameter  $\geq 500$  nm) for the flow cytometer (Table S2, Figure S21). HQ-44, HQ-60, and HQ-100 could not be studied via this method as they formed large nonuniform flocculant aggregates. Fluorescently labeled polyplexes were formed by mixing Cy5-labeled pDNA with the polymers, at  $N/P = 16$ . Next, aggregation of the polyplexes was induced by dilution with FluoroBrite DMEM, consistent with our transfection protocol (Figures 3A and S9–S11). At first, the Cy5 fluorescence intensity ( $\lambda_{\text{ex}} = 651$  nm, and  $\lambda_{\text{em}} = 670$  nm) was used as a parameter to compare the amount of pDNA present in each aggregated polyplex particle. The average Cy5 fluorescence intensity per particle increased with the increase in mole percentage of HQ in the polymer chain (Figure 3B,C), implying a higher amount of pDNA per polyplex particle and corroborating the results from the dye exclusion assay (Figure 2B). Additionally, aggregated polyplexes of QCR showed about 35-fold higher Cy5 fluorescence intensity than that of

HQ-17 despite having a similar polymer composition. This corroborates the results from the dye exclusion assay that the quinine repeat unit has a stronger affinity toward pDNA than the HQ repeat unit, providing further evidence that monomer structure and orientation (Quinine vs HQ) can be tailored to modulate polymer–pDNA binding affinity (Figure 3C).

For engineered nanoparticles, protein adsorption and the resultant protein corona are known to affect their biological fate.<sup>48</sup> Our previous Raman spectroscopic studies have demonstrated that serum proteins are responsible for unpacking of pDNA from polyplexes of QCR.<sup>27,31</sup> To compare the influence of the polymer composition on protein adsorption and cargo unpacking, in the second part of the flow cytometry experiment, the aggregated polyplexes were incubated with fetal bovine serum (FBS), and the changes in the Cy5 fluorescence due to the presence of serum proteins were measured. We observe that introduction of FBS in the polyplex solution led to about 35% decrease in the Cy5 fluorescence intensity from the polyplexes of QCR. This indicates to the protein-mediated release of pDNA from polyplexes, which agrees with our previous results with Raman spectroscopy. In contrast, polyplexes formed with HQ-X showed different characteristics—the polyplex associated Cy5 fluorescence intensity did not change significantly upon the

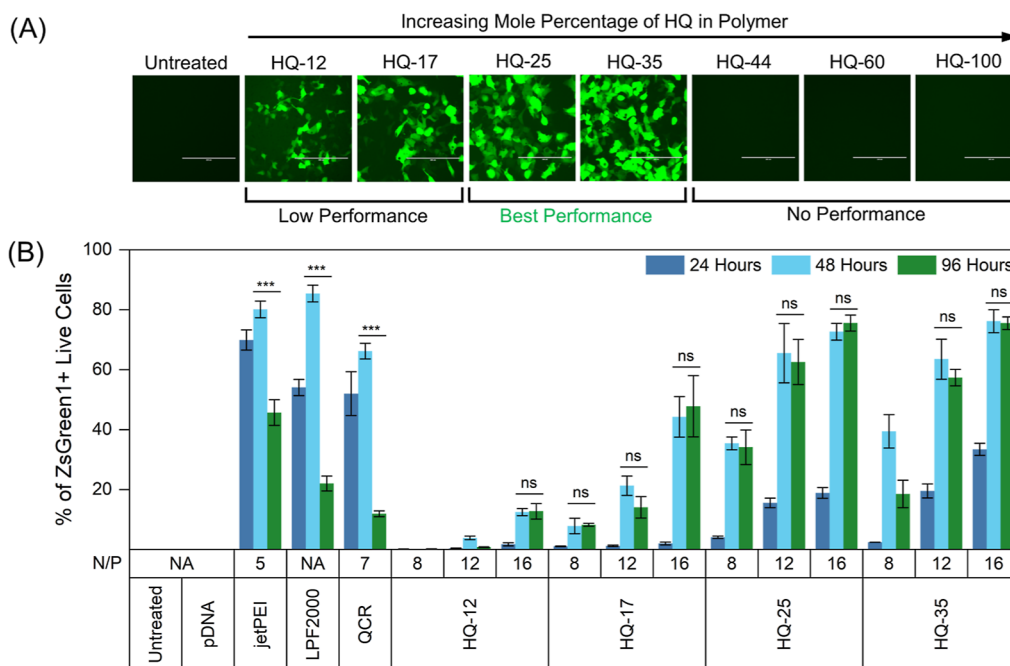


**Figure 4.** (A) Representative widefield fluorescence images of HEK293T cells, 48 h after transfection with pZsGreen1-N1 plasmid,  $N/P = 16$  (scale bar = 200  $\mu\text{m}$ ). Upon successful transfection, the cells produce ZsGreen1 protein that has green fluorescence. (B) Transfection efficiency assessed by quantifying the percentage of live HEK293T cells that are ZsGreen1+, via flow cytometry. Data are the mean of three replicates  $\pm$  standard deviation. Cells transfected using HQ-44, HQ-60, and HQ-100 did not show green fluorescence even at the 96 h time point.

introduction of FBS to the system (Figure 3B,C). This suggests that compared to QCR, polyplexes of HQ-X polymers are less susceptible to protein-mediated unpacking, the influence of which on payload release kinetics is discussed later in the context of sustained effects of transfection.

Finally, to compare the extent of protein adsorption on the polyplexes, we incubated the aggregated polyplexes with Alexa Fluor 488-labeled bovine serum albumin (BSA-AF488) instead of FBS and maintained the same protein concentration as the previous experiment. The fluorescence intensity of Alexa Fluor 488 ( $\lambda_{\text{ex}} = 490 \text{ nm}$ , and  $\lambda_{\text{em}} = 525 \text{ nm}$ ) associated with the aggregated polyplexes was used as an indicator for the amount of protein adsorption. The geometric mean fluorescence intensities from the polyplex particles indicated that polyplexes of HQ-X adsorb less amount of protein relative to polyplexes of QCR (more than a three-fold difference in mean fluorescence intensity) (Figure 3B,D). This explains the difference we observed for changes in Cy5 intensity after the addition of FBS to the polyplexes, i.e., compared to polyplexes of QCR, a significantly less amount of serum protein is adsorbed onto the polyplexes of HQ-12 to HQ-35, and consequently, the degree of pDNA unpacking is also lower (Figure 3C). In other words, polyplexes formed with HQ-X have a lower propensity for protein adsorption and therefore exhibit less unpacking in protein-rich media compared to polyplexes formed with QCR. These observations showcase how subtle differences in the monomer structure and orientation can have great implications on polymer–protein interactions. Overall, this polyplex flow cytometry workflow that we developed has enabled qualitative comparison of different polyplex formulations in three parameters: (i) pDNA loading per polyplex, (ii) adsorption of serum proteins on the polyplexes, and (iii) extent of payload unpacking that is facilitated by serum proteins. These results corroborated our findings from the dye exclusion assay that the polymer–pDNA

binding strength increases with the increase in the mole percentage of HQ in the polymer chain and that for similar molar composition, QCR binds to pDNA more strongly than HQ variants. Additionally, polyplexes of HQ-X adsorb significantly less amount of proteins than QCR, and HQ-X polymers are notably more resilient from protein-mediated payload release.

#### Influence of Composition on the Transfection Efficiency

A goal of this study was also to determine how polymer composition in the HQ-X system influences functional delivery of pDNA into the nucleus and the subsequent expression of the transgene. To evaluate that on an in vitro model, a green fluorescent protein reporter assay was performed using the pZsGreen1-N1 pDNA (4.7 kbp) as the payload. HEK293T cells were transfected with the aggregated polyplex particles formed with HQ-X polymers and pZsGreen1-N1. The transfection efficiency was evaluated based on the percentage of live cells having green fluorescence (i.e., the percentage of live cells producing the green fluorescent protein, ZsGreen1).

With the increase in mole percentage of HQ, the transfection efficiency increased gradually from HQ-12 to HQ-35 but dropped to zero from HQ-44 onward to HQ-100. HQ-25 and HQ-35 emerged as the highest-performing polymers from the HQ-X family with the transfection efficiency reaching about 80%, similar in performance to the commercial controls (jetPEI and Lipofectamine 2000). The complete inability of HQ-44, HQ-60, and HQ-100 to transfect the cells despite having higher  $n_{\text{Hill}}$  and stronger binding with pDNA than the rest of the HQ-X polymers was unexpected (Figures 4A and S12, 13A). The correlation between the transfection efficiency and polymer composition was not monotonic (Figure 4), unlike the trends from dye exclusion assay and potentiometric titration ( $n_{\text{Hill}}$ ). Previous studies have proposed high  $n_{\text{Hill}}$  to be a predictive indicator for high

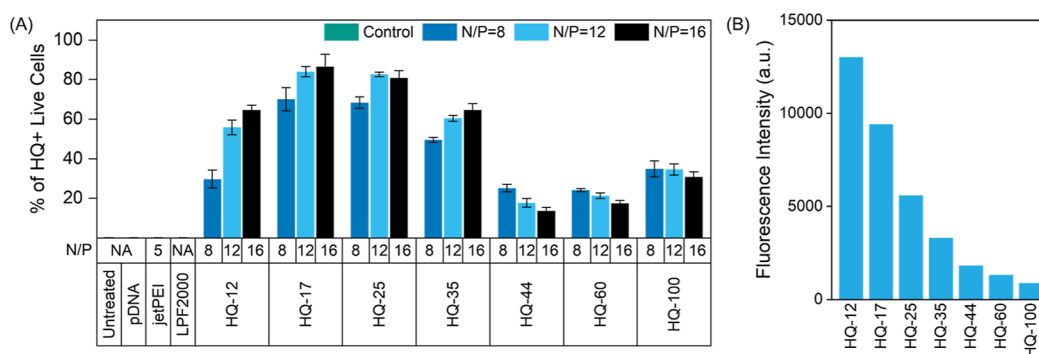


**Figure 5.** (A) Cellular uptake of the polyplexes, measured with flow cytometry, based on the fluorescence intensity of HQ-X observed from the cells. Data are the mean of three replicates  $\pm$  standard deviation. (B) Comparison of fluorescence intensities of HQ-X polymers in 0.05 M acetic acid in water. The amount of polymers in the solution was adjusted for each composition to have [HQ] = 1 mM for all polymers. At lower mole percentages of HQ, the HQ fluorescence can be used to directly quantify the cellular uptake without additional fluorescent tags. However, at higher percentages, self-quenching of HQ fluorescence leads to higher number of false negatives for HQ+ live cells.

transfection performance; however, this clearly does not apply to our HQ-X polymer family. For the HQ-X polymers, electrostatic interactions play a minor role, and the dominant mode of binding between the polymer and pDNA is intercalation which is a non-electrostatic interaction. As a result, the trend in the value of  $n_{\text{Hill}}$  does not explain the trend in the performance of HQ-X polymers as  $n_{\text{Hill}}$  is only relevant for electrostatic interaction. This illustrates that the guiding principles developed for conventional cationic polymers do not necessarily apply to quinine-based polymers (or other monomers with alternative binding mechanisms). Therefore, systematic studies on quinine-based polymers, such as this, are necessary for improving their pDNA delivery efficiency.

An important observation from the transfection results is that compared to QCR, HQ-12 to HQ-35 have a delayed onset of ZsGreen1 expression. Cells transfected using QCR almost reach a maximum transfection efficiency by 24 h; however, HQ-12 to HQ-35 polyplexes require about 48 h to reach the peak efficiency. This slower response with the HQ-X polymers aligns well with the results we obtained by analyzing the protein dependency on unpacking of the polyplexes (Figure 3C,D). Compared to QCR, HQ-X polymers have less affinity to adsorb intracellular proteins and consequently undergo slower unpacking of the payload, ultimately resulting in a delayed onset of ZsGreen1 production. On the other hand, polyplexes of QCR undergo rapid protein-mediated unpacking, leading to a faster cellular response in the form of early onset of ZsGreen1 expression.

For therapeutic applications, a sustained effect of transfection, i.e., gene expression can be useful for reducing the frequency of dose administration.<sup>49,50</sup> To evaluate the ability of HQ-X polymers in sustaining gene expression over a longer period of time, the transfection efficiency was quantified 96 h after transfection, which is 48 h longer than the typical standard in this field (Figures 4B and S14). For QCR and the commercial controls, the ZsGreen1+ population peaked at 48 h but diminished significantly by 96 h. However, for the cells transfected using HQ-17 to HQ-35, the ZsGreen1+ population remained high from 48 to 96 h, outperforming QCR as well as the commercial controls (Figure 4B). We hypothesize that the resistance to protein-mediated unpacking of the polyplexes and consequent slow release of the pDNA payload is responsible for the sustained transfection efficiency observed for HQ-17 to HQ-35. For HQ-44, HQ-60, and HQ-100, fluorescent cells were not observed even 96 h after transfection,

suggesting that for polymers with high HQ content, pDNA release does not occur even after 96 h due to very tight polymer–pDNA association. Overall, these results collectively indicate that the HQ-X class of polymers have more stable pDNA binding characteristics that could benefit packaging, storage, and sustained in vivo delivery for the nucleic acid payload.

### Cellular Uptake Studies

There is literature precedent that cells can internalize particles as large as 5  $\mu\text{m}$  in diameter but generally the extent of the cellular uptake decreases rapidly with an increase in particle size, specifically for particles that are larger than 1  $\mu\text{m}$  in diameter.<sup>51</sup> The larger size and the flocculant nature of the aggregates formed with HQ-44, HQ-60, and HQ-100 (Figure S8, Table S2) were initially hypothesized to be an obstacle for cellular internalization that ultimately rendered them incompatible for transfection. This hypothesis was tested through cellular uptake studies.

At first, we quantified the extent of polyplex internalization (percentage of live cells containing polyplexes) by taking advantage of the inherent fluorescence of the HQ and HQ-X polymers ( $\lambda_{\text{ex}} = 352 \text{ nm}$ ,  $\lambda_{\text{em}} = 460 \text{ nm}$ ) (Figure S15A). We analyzed the cells, 24 h after transfection, using flow cytometry by excitation with an UV laser (350 nm) and observing cells for blue fluorescence. We confirmed the presence of polyplexes from cells that were transfected using HQ-12, HQ-17, HQ-25, and HQ-35. However, we also found polyplexes present inside the cells that were transfected using HQ-44, HQ-60, and HQ-100, although to a relatively lesser extent compared to the other four polymers in the HQ-X family (Figures 5A and S15B). The general trend from this experiment aligned with our initial hypothesis, that polyplexes of HQ-44, HQ-60, and HQ-100 are internalized into the cells to a lesser extent due to their larger size and internalization decreased with increasing composition. The fluorescence of HQ is advantageous in determining the cellular uptake of polyplexes, but it is not without limitations. The fluorescence intensity of HQ-X polymers decreases with an increase in the mole percentage of HQ due to self-quenching (Figure 5B). Therefore, corroborating these results with an additional fluorescent probe was deemed necessary.

To confirm the cellular uptake results, we transfected the cells using Cy5-labeled pDNA and analyzed the cells based on Cy5 fluorescence ( $\lambda_{\text{ex}} = 651 \text{ nm}$ , and  $\lambda_{\text{em}} = 670 \text{ nm}$ ), 24 h after

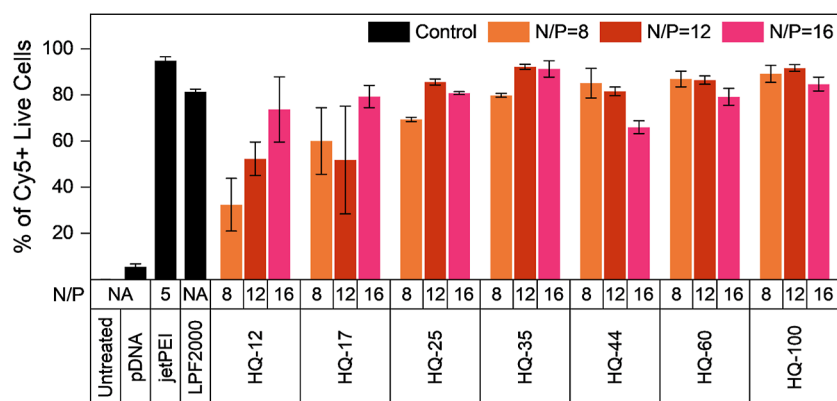


**Figure 6.** Cellular uptake of the polyplexes, measured with flow cytometry, based on the fluorescence intensity of Cy5 (tagged to the pDNA) observed from the cells. Data are the mean of three replicates  $\pm$  standard deviation.

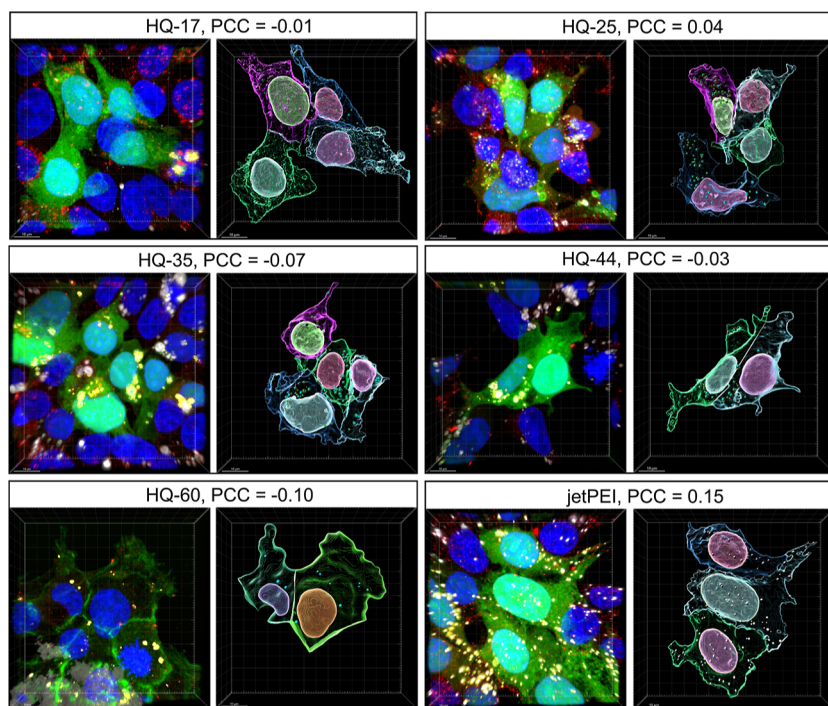


**Figure 7.** Top: representative 3D images (left) and contour surface rendering of the 3D confocal images (right) of HEK293T cells, 24 h after transfection, obtained using confocal laser scanning microscopy. Cy5-labeled pDNA was used as the payload at  $N/P = 16$  (outside cytoplasm: gray, inside cytoplasm: yellow). Lysosomes (red) were stained using an anti-LAMP primary antibody and an Alexa Fluor 555-labeled secondary antibody. Nucleus was stained with DAPI (blue). Fluorescence of ZsGreen1 was used as the cytosolic stain (green). For untreated control, HQ-44, and HQ-60, cell cytoplasm was visualized by staining the actin filaments using Alexa Fluor 488-labeled phalloidin. Pearson's correlation coefficients (PCCs) for colocalization between pDNA and lysosome are mentioned at the top of the respective images. The contour surface renderings were constructed to evaluate distance between nucleus and the Cy5-labeled pDNA present inside the cells. Scale bar 10  $\mu\text{m}$ .

transfection, with flow cytometry (Figures 6 and S16). Cy5 is a more sensitive fluorophore than HQ; therefore, examining the cellular uptake of polyplexes based on Cy5 intensity was expected to have lower occurrences of false negative events than that in the case of HQ fluorescence. The results indicated that all the polymers were able to deliver the Cy5-labeled pDNA inside the cells with half of the formulations achieving more than 80% internalization efficiency (% of Cy5+ live cells), even including most formulations of HQ-44, HQ-60, and HQ-100. Comparing the cellular uptake results from this experiment with the data in Figure 5A, where HQ fluorescence was used, we observe that for HQ-12, HQ-17, and HQ-25, the percentage of Cy5+ cells matches closely with the percentage of HQ+ cells. However, for polymers with a higher mole

percentage of HQ ( $\geq 35\%$ ), the use of HQ fluorescence leads up to 65% underestimation of the cellular uptake due to significant fluorescence quenching of HQ (Figures 5A and 6). With these results, we demonstrate that at low molar incorporation of HQ ( $\leq 25\%$ ), the inherent fluorescence of these polymers can be utilized to directly quantify the extent of the cellular uptake of the polyplexes, without requiring additional fluorescent labeling.

More importantly, it can be concluded that the poor transfection with HQ-44, HQ-60, and HQ-100 is not due to the limitation on the internalization of the polyplexes as a result of their size or flocculant nature. Based on the combined results of dye exclusion assays, polyplex flow cytometry, cellular uptake, and transfection experiments, it appears that for HQ-

44, HQ-60, and HQ-100, the primary obstacle in successful transfection and the subsequent gene expression is the insufficient release of pDNA from the polyplexes after internalization into the cytoplasm. For successful transfection and transgene expression, the pDNA needs to be released from the polyplexes inside the cell and get translocated into the nucleus. Polymers with a high mole percentage of HQ ( $\geq 44\%$ ) likely bind too strongly with pDNA not allowing it to be released from the polyplexes inside the cytoplasm, preventing its translocation to the nucleus, and production of ZsGreen1. Though QCR binds to pDNA as tightly as HQ-44, HQ-60, and HQ-100, a higher affinity for proteins allows the pDNA to be released from polyplexes of QCR making it functional. On the other hand, at lower percentages of HQ ( $\leq 17\%$ ), the binding between pDNA and the polymer is not sufficient to form stable polyplexes, resulting again in the poor transfection efficiency. Based on the transfection results, it can be concluded that mole percentages between 25% and 35% for HQ provide the optimum balance between polymer–pDNA binding and post-internalization pDNA release. This trend highlights the importance of the balance of binding and release of the genetic payload that has strong literature precedent.<sup>52–54</sup>

#### Evaluating Endosomal Escape with Colocalization Studies

To gain insights into the subcellular localization and intracellular behavior of the polyplexes, we performed colocalization experiments using confocal laser scanning microscopy on fluorescently labeled HEK293T cells. The cells were transfected with five out of the seven polymers from the HQ-X family (HQ-17, HQ-25, HQ-35, HQ-44, and HQ-60) using Cy5-labeled pZsGreen1-N1 pDNA as the payload. 24 h after transfection, the cells were fixed, and the lysosomal-associated membrane protein-2 (LAMP2) were stained with a primary antibody and an Alexa Fluor 555-labeled secondary antibody. The colocalization of pDNA (Cy5) and lysosome (Alexa Fluor 555) was evaluated in the form of Pearson's correlation coefficient (PCC) (Figures 7 and S17). For all five polymers, the PCC score was found to be close to zero (between  $-0.1$  and  $0.1$ ), implying that there is no correlation in the localization of the pDNA payload and the lysosomes. This suggests that all five of the HQ-X polymers that were tested were able to facilitate endosomal escape of the pDNA payload from endosomal compartments, and it aligns well with the fact that HQ is structurally and physiochemically similar to chloroquine, a well-known endosomal escape enhancer. Due to having low  $pK_a$  (Table 1), the large reserves of unprotonated amines in the HQ-X polymers likely act like a proton sponge and facilitate endosomal escape. As a comparison, the PCC score from the jetPEI-treated cells was higher (0.15) than the cells transfected using HQ-X, which further highlights the ability of HQ-X polymers for endosomal escape (Figure S18). Furthermore, the low PCC scores for HQ-44 and HQ-60, which is the proof of efficient endosomal escape of pDNA, strengthens the hypothesis we proposed earlier that the poor release of pDNA from the polyplexes is the primary bottleneck against productive transfection for polymers with high HQ content ( $\geq 44\%$ ). We also compared the distribution of the distances between the internalized Cy5-labeled pDNA and the nuclear membrane and found that HQ-17, HQ-25, and HQ-35 are able to shuttle pDNA 20–30% closer to the nuclear periphery than HQ-44 and HQ-60 (Figure S19). Our hypothesis on poor release of pDNA from HQ-44, HQ-60, and HQ-100 was further validated by performing a dye

exclusion assay in the presence of heparin which is a polyanion known to compete with pDNA to bind with cationic polymers (Figure S23).<sup>55</sup> We observed that the extent of pDNA release from polyplexes, caused by heparin, decreases with the increase in the HQ content of the polymer clearly indicating that among the HQ-X polymers, HQ-44, HQ-60, and HQ-100 not only bind with pDNA the strongest but also have the least amount of pDNA release. Overall, results obtained from the confocal microscopy experiment showcase the endosomal escape capabilities of the HQ-X polymers and provide further evidence to our hypothesis that at high molar incorporation of HQ, the major bottleneck in transfection is related to poor unpackaging and release of the pDNA rather than cellular internalization and trafficking.

#### CONCLUSIONS

In our pursuit of developing highly efficient polymer-based gene delivery vehicles, we have synthesized and studied in detail a collection of polymers based on quinine, a promising natural product from the cinchona alkaloid family. The challenges of polymerizing quinine were circumvented by using a hydroquinine-functionalized monomer, HQ. The compatibility of HQ toward RAFT copolymerization as well as free-radical homopolymerization allowed a great degree of control in synthesizing copolymers of desired molar composition (HQ content: 12–100%) and molar mass. We also developed an assay for analyzing polyplex particles using a flow cytometer and demonstrated the influence of the polymer composition as well as the monomer structure on three key features of polyplexes: the amount of pDNA loaded per polyplex particle, the extent of protein adsorption on the particles, and the protein-mediated release of pDNA from the particles. Although the polymer–pDNA binding increased monotonically with the percentage of HQ in the polymer, the maximum transfection efficiency in cellular studies was achieved with 25% and 35% incorporation of HQ (HQ-25 and HQ-35, respectively)—the optimum range of the composition needed for balancing pre-internalization pDNA binding and post-internalization pDNA release. HQ-25 and HQ-35 also showed superiority over QCR as well as the standard transfection agents, jetPEI and Lipofectamine 2000, in terms of sustaining the effect of transfection over 96 h. Quantitative confocal microscopy and image analysis establish the remarkable endosomal escape capability of HQ-X polymers, eliminating the need for endosome disrupting agents such as chloroquine. The results also support our hypothesis that polymers with high molar incorporation of HQ do not transfect well, likely due to poor release of pDNA from the polyplexes inside the cells. Overall, in this work, we have developed quinine-based polymers possessing excellent gene delivery efficiency with the ability to sustain transgene production and great endosomal escape capability and also showcased fundamental guiding principles on using non-electrostatic interactions such as intercalation to our advantage for modulating polymer–pDNA binding. These results will serve as a stepping stone toward developing the next generation of natural product-based polymers for delivery of therapeutic nucleic acids of different kinds, both single as well as double stranded, such as antisense oligonucleotides (ASO), siRNA, mRNA, and even Cas9-sgRNA complexes for gene editing.

## MATERIALS AND METHODS

### Synthesis

Quinine (anhydrous, 99% total base with  $\leq 5\%$  dihydroquinine) was purchased from Alfa Aesar (Tewksbury, MA). Hydroquinine (98%), HEA, 4-cyano-4-[(dodecylsulfanylthiocarbonyl)sulfanyl]pentanoic acid, 2-(dodecylthiocarbonothioylthio)-2-methylpropionic acid (DDMAT), azobisisobutyronitrile (AIBN), 4,4'-azobis(cyanovaleric acid) (V-501), silica gel (technical grade, pore size 60 Å, 70–230 mesh), and heparin ammonium salt from porcine intestinal mucosa were purchased from Sigma-Aldrich (St. Louis, MO). 2-Isocyanatoethyl acrylate (stabilized with BHT (butylated hydroxytoluene)) was purchased from TCI Chemicals (Portland, Oregon). Spectra/Por Pre-wetted RC dialysis tubing (MW cutoff  $\sim 1$  kDa) was purchased from Spectrum Chemical Mfg. Corp (New Brunswick, NJ). The tubing was soaked in and rinsed with Milli-Q water prior to use.

### Transfection

The pZsGreen1-N1 plasmid DNA (4.7 kbp) was purchased from Aldevron (Fargo, ND). The CCK-8 cell counting kit was purchased from Bimake (Houston, TX). Lipofectamine 2000, SYTOX red dead cell stain, and PicoGreen (Quant-iT PicoGreen, dsDNA reagent) were purchased from Thermo Fisher Scientific (Waltham, MA). CellScrub buffer was purchased from Genlantis (San Diego, CA). Label IT Nucleic Acid Labeling Kit, Cy5 was purchased from Mirus Bio (Madison, WI). jetPEI was purchased from Polyplus-transfection (New York, NY).

### Cell Culture

Dulbecco's Modified Eagle's Medium (DMEM; high glucose, pyruvate, and GlutaMAX supplemented), FluoroBrite DMEM, Trypsin-EDTA (0.05%) with and without phenol red, phosphate-buffered saline (PBS) pH = 7.4, UltraPure DNase/RNase-free distilled water (DI H<sub>2</sub>O), antibiotic–antimycotic (100 $\times$ ), and flow cytometry sub-micron particle size reference kit (F13839) were purchased from Life Technologies Thermo Fisher Scientific (Carlsbad, CA). Heat-inactivated fetal bovine serum (HI FBS) was purchased from Corning Life Sciences (Durham, NC). Cell lines of human embryonic kidney cells (HEK293T) were engineered from the laboratory of Mark Osborne at the University of Minnesota with a traffic light reporter system. Subclones were made at the Genome Engineering Shared Resource (Minneapolis, MN) to obtain a stable cell line.

### Microscopy

For confocal microscopy imaging, cells were plated in eight-well chambered slides purchased from ibidi (Gräfelfing, Germany). Anti-LAMP2 antibody [H4B4]—lysosome marker and normal goat serum was purchased from Abcam (Waltham, MA). Goat anti-Mouse IgG (H + L) highly cross-adsorbed secondary antibody, Alexa Fluor 555, and SlowFade Glass (with DAPI) Soft-set antifade mountant were purchased from Invitrogen (Thermo Fisher Scientific; Waltham, MA). Gelatin from porcine skin (gel strength  $\sim 300$  g Bloom) and BSA were purchased from Sigma (St. Louis, MO). 16% Paraformaldehyde aqueous solution was purchased from Electron Microscopy Sciences (Hatfield, PA). Triton X-100 was purchased from Integra (Renton, WA). The Steriflip vacuum-driven filtration system (0.22  $\mu\text{m}$ ) was purchased from Millipore (Burlington, MA).

### Instrument Details

NMR spectra were recorded on AX-400 Bruker Avance III HD (Billerica, MA). Mass spectra were recorded on a BioTOF II ESI-TOF Mass Spectrometer. Size exclusion chromatography was performed on the Agilent Infinity 1260 HPLC system equipped with the Wyatt DAWN Heleos II multiangle laser light scattering detector and Wyatt OPTILAB T-rEX refractive index detector. Molar masses were obtained using  $dn/dc$  values calculated from the refractive index signal using samples with the known concentration with an assumption of 100% mass recovery. Absorbance and fluorescence measurements of polymers and polyplexes were acquired using the Synergy H1 multimode plate reader (BioTek; Winooski,

VT). pH measurements and potentiometric titrations were carried out with OrionStar T910 (Thermo Fisher Scientific; Waltham, MA). Flow cytometry was performed on a ZES5 cell analyzer (Bio-Rad; Hercules, CA), and results were analyzed using FlowJo software (Ashland, OR). DLS measurements were made with a Zetasizer Nano ZS (Malvern; Worcestershire, UK) with a 4.0 mW He–Ne laser ( $\lambda = 633$  nm). Cell suspensions were counted with a Countess II automated cell counter (Thermo Fisher Scientific; Waltham, MA) with dead cell discrimination by dilution (1:1) with trypan blue (0.4%). Widefield fluorescence microscopy was carried out using an EVOS Digital Microscope (AMG Life Technologies; Grand Island, NY). Confocal microscopy images were acquired on Olympus Fluoview FV1000 BX2 Upright Confocal. All statistical calculations were performed with GraphPad Prism v9.4.1.

### Synthesis of HQ

In a round-bottom flask, hydroquinine (4.0 g, 12.3 mmol) was dissolved in anhydrous THF (50 mL) followed by addition of dibutyltin dilaurate (23 mg, 0.036 mmol dissolved in 5 mL of anhydrous THF) into the reaction mixture.<sup>37</sup> A solution of 2-isocyanatoethyl acrylate (2.3 g, 16 mmol) in anhydrous THF (20 mL) was added dropwise to the reaction mixture under continuous stirring. After stirring for 30 min at room temperature, the reaction mixture was heated to 40 °C in an oil bath and was stirred for another 24 h under a N<sub>2</sub> atmosphere. Completion of the reaction was confirmed via TLC, and excess 2-isocyanatoethyl acrylate was quenched by adding distilled water. The quenched reaction mixture was washed with ethyl acetate (3  $\times$  200 mL) to extract the product into the organic phase. The organic phase was further washed with brine, followed by drying over anhydrous Na<sub>2</sub>SO<sub>4</sub>, and then was concentrated under vacuum. The pure product was isolated by flash chromatography using silica gel as the stationary phase and 20% methanol in DCM as the mobile phase. The purified product was dried under high vacuum overnight before further use.

### Polymerization of HQ via Reversible Addition–Fragmentation Chain-Transfer Polymerization (RAFT)

Into one-dram vials, monomers (HQ and HEA), chain-transfer agent (DDMAT), and initiator (AIBN) were transferred and dissolved in anhydrous DMF (total monomer concentration = 1 M, [total monomer]/[DDMAT]/[AIBN] = 200:1:0.2). The vials were closed with the Suba-Seal septa, and the reaction mixture was purged with N<sub>2</sub> for minimum of 30 min. Subsequently, the vials were transferred to the metal heating block and stirred vigorously for 6 h at 80 °C. The reactions were quenched by rapidly cooling the reaction mixture in liquid N<sub>2</sub> bath followed by exposure to atmospheric oxygen. The reaction mixture was diluted with 10% THF (inhibitor free) in methanol, then transferred to RC dialysis tubing, and then dialyzed for 4 days using 10% THF (inhibitor free) in methanol. The purified polymer solutions were first concentrated under vacuum and then dried under high vacuum overnight to yield the pure polymer. For all experiments and assays, polymer stock solutions were prepared in 3% acetic acid in water solution. The polymer solutions were vortexed well and then filtered using a 0.22  $\mu\text{m}$  syringe filter before use.

### Polymerization of HQ via Free-Radical Polymerization (FRP)

Into one-dram vials, HQ (with or without HEA) and AIBN were loaded and dissolved in anhydrous DMF. Total monomer concentration was 1 M with [total monomer]/[AIBN] ratio being 100:1. The vials were closed with Suba-Seal septa, and the reaction mixture was purged with N<sub>2</sub> for minimum of 30 min. After that, the vials were placed in metal blocks and stirred in the N<sub>2</sub> atmosphere at 80 °C for 15 h. The polymerization reactions were quenched by rapidly cooling the reaction mixture in liquid N<sub>2</sub> baths and then exposing them to atmospheric oxygen. The reaction mixture was diluted with 10% THF (inhibitor free) in methanol, then transferred to RC dialysis tubing, and then dialyzed for 4 days in 10% THF (inhibitor free) in methanol. The purified polymer solutions were first concentrated under vacuum and then dried under high vacuum

overnight to yield the pure polymer. For all experiments and assays, the polymer stock solution was prepared in 3% acetic acid in water solution. The polymer solution was vortexed well and then filtered using a 0.22  $\mu\text{m}$  syringe filter before use.

### Potentiometric Titration

Monomers and polymers were dissolved in 30 mM HCl to prepare 15 mL of stock solutions having concentration of 1 mg/mL. This acidic solution was titrated with freshly prepared 75 mM NaOH solution, using the OrionStar autotitrator, under constant stirring. The titration endpoints were determined from the derivative of the titration curve. A linear fit was applied between the titration endpoints, and the  $\text{pK}_a$  values were calculated by determining the pH at the middle point of the titration endpoints. Hill coefficients were calculated by rearranging the titration curve data into eq 1 and plotting  $\log \frac{\theta}{1-\theta}$  vs  $\text{pK}_a - \text{pH}$  and applying linear fit.

$$\log \frac{\theta}{1-\theta} = n_{\text{Hill}} \cdot (\text{pK}_a - \text{pH}) \quad (1)$$

According to eq 1,  $\theta$  is the fraction of amines protonated and  $n_{\text{Hill}}$  is the Hill coefficient which was determined from the slope of the  $\log \frac{\theta}{1-\theta}$  vs  $\text{pK}_a - \text{pH}$  plot.

### Dye Exclusion Assay

To improve the aqueous solubility of the polymers as well as to increase the electrostatic interactions between the polymer chains and the pDNA, the stock solutions for the polymers were prepared in aqueous solution of acetic acid (3% glacial acetic acid in water,  $\text{pH} \sim 2.6$ ), similar to our previous work with QCR.<sup>31</sup> In general, for all experiments and assays, stock solutions of the polymer (0.0104 M with respect of quinuclidine nitrogen atoms) and pDNA (1 mg/mL) were diluted with ultrapure water to freshly prepare secondary solutions with appropriate concentrations. pDNA was always diluted to 0.02 mg/mL, and the polymer solutions were diluted according to the desired  $N/P$  of the final mixture. For the dye exclusion assay, pDNA was diluted with ultrapure water that was doped with PicoGreen (0.5% v/v). The polymer secondary solution was added into the pDNA secondary solution in a 1:1 volume ratio to form primary polyplexes for 30 min at room temperature. Fluorescence intensity was measured using the fluorescence filter cube ( $\lambda_{\text{ex}} = 485/20$  nm, and  $\lambda_{\text{em}} = 528/20$  nm). The intensity from polyplex solutions (at respective  $N/P$  ratios) without PicoGreen was used for background subtraction. The intensity from the polymer-free solutions ( $N/P = 0$ ) was used to normalize the intensity from polyplex solutions. Additionally, fluorescence of the polymers in the presence of PicoGreen but without pDNA was measured for which we only observed the baseline level fluorescence signal. These controls confirmed that neither the fluorescence of the free polymer nor the interaction of PicoGreen with polymer interferes with the dye exclusion results.

The ability of the polymers to release pDNA after formation of polyplexes was tested with a modified version of dye exclusion with the addition of heparin at the final concentration of 33.5  $\mu\text{g}/\text{mL}$ .<sup>55</sup> Control samples were prepared by adding water instead of heparin to the polyplex solution. The difference in normalized fluorescence intensity due to addition of heparin was used to compare the extent of pDNA release from polyplexes in the presence of heparin (Figure S23).

### Flow Cytometry on Aggregated Polyplexes

To determine the lower size limit of detection for the polyplex particles, commercially available fluorescent particles with diameters of 100, 200, 500, 1000, and 2000 nm were used first on the flow cytometer. Forward scattering intensity and green fluorescence intensity were used in tandem to distinguish the particles from noise. From this study, the lower detection limit was found to be 500 nm in diameter (Figure S21). Fluorescently labeled primary polyplex particles were formed using the general protocol described for dye exclusion assay but with the modification of using Cy5-labeled pZsGreen1-N1 pDNA. The primary polyplex solutions were diluted

in 1:2 volume ratio using FluoroBrite DMEM to induce aggregation of the polyplexes. The aggregated polyplex solutions were split into three portions. The first portion was left untreated, the second portion was treated with 10% FBS, and the third portion was treated with FBS doped with BSA conjugated with Alexa Fluor 488 (95% FBS + 5% BSA-AF488). Aggregated polyplexes were also formed with unlabeled pZsGreen1-N1 pDNA to serve as controls.

### Cell Culture

The engineered HEK293T cells were cultured in DMEM supplemented with 10% FBS and 1% antibiotic–antimycotic at 37 °C and 5%  $\text{CO}_2$  in 75  $\text{cm}^2$  cell culture flasks.

### Transfection

Cells were plated in 24-well plates at the density of 50,000 cells/mL, 24 h before transfection. Manufacturer's protocol was used for transfection with jetPEI and Lipofectamine 2000. For HQ-X polymers as well as QCR, previously reported transfection protocol was used with minor modifications.<sup>31</sup> Similar to the protocol mentioned for dye exclusion assay and flow cytometry on polyplexes, secondary solutions of polymer and pDNA were mixed in a 1:1 volume ratio and incubated for 30 min at room temperature to form primary polyplexes at the desired  $N/P$  ratios. The polyplex solutions were then diluted in a 1:2 volume ratio using FluoroBrite DMEM to induce aggregation of the polyplexes. After 30 min, the cells were washed with PBS and treated with the aggregated polyplex solution with each well receiving 1  $\mu\text{g}$  of pDNA. The cells were then incubated at 37 °C with 5%  $\text{CO}_2$  for 30 min before addition of 1 mL of serum-supplemented DMEM into each well. Fresh supplemented media was added to each well 24 h later. Negative controls were performed with cells being similarly treated with media that is equivalently diluted but does not contain any polymer and pDNA to confirm that the cells are tolerant of the media changes, the wash procedures, and the duration of transfection. Transfection in the presence of serum was also tested using HQ-25 as a model polymer, at  $N/P = 12$ . To transfect the cells, aggregated polyplexes were prepared according to the regular transfection protocol followed by addition of polyplex solution directly into serum-supplemented media (Figure S22).

### Quantifying Cell Viability

Cell viability was measured using colorimetric assay with CCK-8. 48 h after transfection, the cells were treated with 6% solution of CCK-8 in FluoroBrite DMEM and incubated at 37 °C with 5%  $\text{CO}_2$  for 1 h. After 1 h, the supernatant solution was transferred to a clear 96-well plate, and the absorbance of the supernatant solution at 450 nm was measured. Absorbance from 6% CCK-8 solution in FluoroBrite DMEM was subtracted from all data points, and the values were normalized to the absorbance from the supernatant of untreated cells (Figure S13B).

### Quantifying Transfection Efficiency with Flow Cytometry

48 h after transfection, the cells were washed with warm PBS and trypsinized using phenol red-free trypsin for 5 min followed by quenching of trypsinization with serum-supplemented phenol red-free DMEM. The cell suspension was diluted with ice-cold PBS containing 2% FBS and centrifuged at 4 °C at 1000 rpm for 10 min in deep well plates. The supernatant was discarded, and the cells were resuspended in ice-cold PBS with 2% FBS and 17 nM SYTOX Red and used for flow cytometry. Untreated cells were used as negative controls for gating. 350, 488, and 640 nm lasers were used for detecting HQ+, ZsGreen1+, and SYTOX Red+ cells, respectively (Figure S12).

For quantifying the effect of transfection 96 h after the transfection, a separate transfection was performed following the same protocol. 48 h after transfection, the cells were passaged and plated into a new 24-well plates with 1:3 split to allow continuous growth. The media was changed 24 h later. After a total of 96 h, the cells were prepared for flow cytometry following the protocol mentioned earlier.

### Labeling pDNA with Cy5

The label-IT nucleic acid labeling kit from Mirus Bio was used to prepare Cy5-labeled pDNA using manufacturer's protocol with one adjustment. Briefly, one full kit was used to label 1 mg of pDNA

instead of 100  $\mu\text{g}$ . The reduction in labeling density was to minimize alteration in polymer–pDNA binding while keeping sufficient number of fluorophores for detection using flow cytometry and confocal microscopy. Labeling density of the fluorescent probe was calculated using the spectrophotometric method provided by Mirus Bio. The average ratio of nucleobase to Cy5 was calculated to be 440 which implies that each pDNA was labeled with 21 molecules of Cy5 on average.

### Polyplex Internalization Measurement Using Cy5-Labeled pDNA

Cells were transfected according to the typical protocol using the Cy5-labeled pZsGreen1 plasmid. 24 h after transfection, the cells were washed PBS and trypsinized using phenol red-free trypsin for 5 min followed by quenching of trypsinization with serum-supplemented phenol red-free media. The cell suspension was diluted with ice-cold PBS containing 2% FBS and centrifuged at 4  $^{\circ}\text{C}$  at 1000 rpm for 10 min in deep well plates. The supernatant was removed, and the cells were incubated with CellScrub solution for 10 min at room temperature followed by centrifugation at 4  $^{\circ}\text{C}$  at 1000 rpm for 10 min. The supernatant was discarded, and the cells were resuspended in ice-cold PBS with 2% FBS and used for flow cytometry measurements. 640 nm laser was used for detecting Cy5<sup>+</sup> cells, and 350 nm laser was used detecting HQ<sup>+</sup> cells.

### Confocal Microscopy

The general transfection protocol was followed, but the amounts of reagents were reduced by half. Fluorescent labels were carefully selected to provide sufficient spectral separation during image acquisition. Cy5-labeled pZsGreen1-N1 was used as the payload. 24 h before transfection, eight-well chambered slides were coated with porcine gelatin solution (0.1%) followed by seeding with HEK293T cells with concentration of 25,000 cells/well. For transfection with jetPEI, *N/P* of 5 was used. For HQ-X polymers, *N/P* = 16 was used. 24 h after transfection, the cells were washed gently with PBS followed by fixation with 4% paraformaldehyde in PBS for 15 min at room temperature. After fixation, the fixative solution was discarded, and the cells were washed gently with PBS followed by permeabilization with washing buffer (0.1% Triton-X100 in PBS for 5 min). The washing buffer was then switched with blocking buffer (5% BSA, 1% normal goat serum, and 0.1% Triton-X100 in PBS), and the cells were kept submerged in blocking buffer for 60 min at room temperature. Subsequently, the blocking buffer was switched with primary antibody solution (anti-LAMP2 antibody [H4B4] diluted 1:200 in blocking buffer), and the cells were kept submerged in it overnight at 4  $^{\circ}\text{C}$ . The following day, the primary antibody solution was discarded, and the cells were washed with washing buffer before treatment with secondary antibody solution [goat anti-mouse IgG (H + L) highly cross-adsorbed secondary antibody Alexa Fluor 555 diluted 1:1000 in blocking buffer] for 60 min. Next, the secondary antibody solution was discarded, and the cells were washed with washing buffer. Residual buffer was removed carefully, and the glass coverslip was mounted on top of the cells using SlowFade Glass (with DAPI) as the mountant, and the cells were imaged on the same day. The fluorescent profile of HQ matches with DAPI, but the overall brightness of HQ is significantly lower than DAPI to be able to interfere in confocal imaging. Furthermore, the DAPI staining was used for cell segmentation during the image processing, and it is not connected to calculations for PCC which provided us the most meaningful insight from confocal microscopy images.

All images were collected on an Olympus Fluoview 1000 BX2 upright confocal imaging system equipped with a Prior stage controller, lasers, primary dichromatic mirror, emission filters, photomultiplier tube detectors, and a PLAPON 60 $\times$  oil objective (NA 1.42). Laser illumination consisted of 405 and 635 nm solid-state diode lasers set to 20 and 50% laser power, respectively, a 543 nm HeNe laser set to 60% laser power, and a 488 nm argon laser set to 15% laser power. The dichromatic mirrors for the various channels consisted of a SDM490 mirror for the DAPI channel, a SDMS60 mirror for the Alexa Fluor 488 channel, and a SDM640 mirror for the

Alexa Fluor 555 channel. Emission bandpass filters ranged from 450/40 nm for blue emission, 515/20 nm for green emission, 610/100 nm for orange-red emission, to 705/100 nm for far red emission. Voltage settings for the photomultiplier tube detectors were 555 V with an offset of 7 for the DAPI channel, 470 V with an offset of 6 for the Alexa Fluor 488 channel, 705 V with an offset of 7 for the Alexa Fluor 555 channel, and 535 V with an offset of 4 for the Cy5 channel. Acquisition software was controlled by FluoView FV1000 software, version 4.1.1.5 (Waltham, Massachusetts).

### Confocal Microscopy Image Analysis

All images were collected in the Olympus Image Binary format and converted to TIFF images, which were imported into Nikon Elements Analysis software (version 5.41.01) for spectral unmixing. Labeling nuclei with DAPI inadvertently stained the Cy5-labeled pDNA as well, this had to be spectrally unmixed with Nikon Elements software using the ROI method, and the unmixed images were saved as ND2 files. These files were next converted into IMS files with Imaris FileConverter (version 9.9.1) for eventual processing, segmentation, and quantification in Imaris software (version 9.9.1). First, background was automatically subtracted from all images with a Gaussian filter radius of 17.6 to define the background at each voxel, and then, software conducted a baseline subtraction of this variable background. Structures smaller than the automatically calculated filter width were removed. Second, all images were smoothed and denoised with a 3  $\times$  3  $\times$  3 median filter. Segmentation of nuclei and cells employed the surface module. First DAPI-stained nuclei were automatically thresholded and segmented by morphological split with an estimated region growing diameter of 5.0  $\mu\text{m}$ . Next, cells were detected via expression of ZsGreen1 and manually thresholded, followed by segmentation by morphological split with an estimated region growing diameter of 8.0  $\mu\text{m}$ . Cy5-labeled pDNA (Cy5-pDNA) was detected and segmented with the spot module. Region growing detection and local contrast were enabled, and spot sizes were estimated as 0.6  $\mu\text{m}$  laterally and 1.76  $\mu\text{m}$  axially followed by manual thresholding. These surface and spot renderings were imported into the cell module, wherein Cy5-pDNA distances to the nucleus border were measured. In Imaris software, lysosome–Cy5-labeled pDNA colocalization was measured within the cell boundaries imposed by ZsGreen1 labeling. Lysosome and Cy5 signals were automatically thresholded with the method devised by Costes et al.<sup>56</sup> A colocalization channel was built from which PCCs were calculated. PCCs within the colocalized volume were utilized for data analysis.

## ■ ASSOCIATED CONTENT

### Supporting Information

The Supporting Information is available free of charge at <https://pubs.acs.org/doi/10.1021/jacsau.3c00126>.

Characterization data for monomers and polymers, DLS, transfection, flow cytometry, and confocal image analysis (PDF)

## ■ AUTHOR INFORMATION

### Corresponding Author

Theresa M. Reineke – Department of Chemistry, University of Minnesota, Minneapolis, Minnesota 55455, United States; [orcid.org/0000-0001-7020-3450](https://orcid.org/0000-0001-7020-3450); Email: [treineke@umn.edu](mailto:treineke@umn.edu)

### Authors

Punarbassu Roy – Department of Chemistry, University of Minnesota, Minneapolis, Minnesota 55455, United States; [orcid.org/0000-0001-8937-7856](https://orcid.org/0000-0001-8937-7856)

Nicholas W. Kreofsky – Department of Chemistry, University of Minnesota, Minneapolis, Minnesota 55455, United States

Mary E. Brown – University Imaging Centers, University of Minnesota, Minneapolis, Minnesota 55455, United States  
Craig Van Bruggen – Department of Chemistry, University of Minnesota, Minneapolis, Minnesota 55455, United States

Complete contact information is available at:  
<https://pubs.acs.org/10.1021/jacsau.3c00126>

### Author Contributions

CRedit: **Punarbazu Roy** conceptualization, formal analysis, investigation, methodology, validation, visualization, writing-original draft, writing-review & editing; **Nicholas Kreofsky** conceptualization, formal analysis, investigation, methodology, validation, writing-original draft, writing-review & editing; **Mary E. Brown** formal analysis, investigation, methodology, visualization; **Craig Van Bruggen** conceptualization, investigation; **Theresa M. Reineke** conceptualization, funding acquisition, investigation, methodology, project administration, supervision, writing-original draft, writing-review & editing.

### Notes

The authors declare no competing financial interest.

### ACKNOWLEDGMENTS

We thank Dr. Bockman and Dr. Santa Chalarca for valuable suggestions in monomer and polymer synthesis. This work was supported by the resources and staff at the University of Minnesota University Imaging Centers (UIC) (SCR\_020997). N.W.K. acknowledges funding under the NSF Graduate Research Fellowship Program (DGE-2237827) and the 3M Science and Technology Graduate Fellowship (University of Minnesota). The image acquisition and image analysis were performed by UIC staff member M.E.B. This work was funded by the NSF (DMR-1904853, P.R., N.W.K., and T.M.R.). Figures were created with [BioRender.com](https://BioRender.com).

### REFERENCES

- (1) Bulaklak, K.; Gersbach, C. A. The Once and Future Gene Therapy. *Nat. Commun.* **2020**, *11*, 5820–5914.
- (2) Goswami, R.; Subramanian, G.; Silayeva, L.; Newkirk, I.; Doctor, D.; Chawla, K.; Chattopadhyay, S.; Chandra, D.; Chilukuri, N.; Betapudi, V. Gene Therapy Leaves a Vicious Cycle. *Front. Oncol.* **2019**, *9*, 1–25.
- (3) High, K. A.; Roncarolo, M. G. Gene Therapy. *N. Engl. J. Med.* **2019**, *381*, 455–464.
- (4) Dunbar, C. E.; High, K. A.; Joung, J. K.; Kohn, D. B.; Ozawa, K.; Sadelain, M. Gene Therapy Comes of Age. *Science* **2018**, *359*, No. eaan4672.
- (5) American Society of Gene & Cell Therapy. Gene, Cell, and RNA Therapy Landscape. Q4 2022 Quarterly Data Report, [https://asgct.org/global/documents/asgct\\_citeline-q4-2022-report\\_final.aspx](https://asgct.org/global/documents/asgct_citeline-q4-2022-report_final.aspx) (accessed 27 Feb, 2023).
- (6) Ginn, S. L.; Amaya, A. K.; Alexander, I. E.; Edelstein, M.; Abedi, M. R. Gene Therapy Clinical Trials Worldwide to 2017: An Update. *J. Gene Med.* **2018**, *20*, e3015–e3016.
- (7) Sheridan, C. To Win at Gene Therapy, Companies Pick Viruses with Production Credentials. *Nat. Biotechnol.* **2019**, *37*, 5–6.
- (8) Lee, C. S.; Bishop, E. S.; Zhang, R.; Yu, X.; Farina, E. M.; Yan, S.; Zhao, C.; Zeng, Z.; Shu, Y.; Wu, X.; Lei, J.; Li, Y.; Zhang, W.; Yang, C.; Wu, K.; Wu, Y.; Ho, S.; Athviraham, A.; Lee, M. J.; Wolf, J. M.; Reid, R. R.; He, T.-C. Adenovirus-Mediated Gene Delivery: Potential Applications for Gene and Cell-Based Therapies in the New Era of Personalized Medicine. *Genes Dis.* **2017**, *4*, 43–63.
- (9) Li, C.; Samulski, R. J. Engineering Adeno-Associated Virus Vectors for Gene Therapy. *Nat. Rev. Genet.* **2020**, *21*, 255–272.
- (10) Wu, Z.; Yang, H.; Colosi, P. Effect of Genome Size on AAV Vector Packaging. *Mol. Ther.* **2010**, *18*, 80–86.
- (11) Thomas, C. E.; Ehrhardt, A.; Kay, M. A. Progress and Problems with the Use of Viral Vectors for Gene Therapy. *Nat. Rev. Genet.* **2003**, *4*, 346–358.
- (12) Bessis, N.; GarciaCozar, F. J.; Boissier, M.-C. Immune Responses to Gene Therapy Vectors: Influence on Vector Function and Effector Mechanisms. *Gene Ther.* **2004**, *11*, S10–S17.
- (13) Chaudhary, N.; Weissman, D.; Whitehead, K. A. MRNA Vaccines for Infectious Diseases: Principles, Delivery and Clinical Translation. *Nat. Rev. Drug Discovery* **2021**, *20*, 817–838.
- (14) Kumar, R.; Santa Chalarca, C. F.; Bockman, M. R.; Bruggen, C. V.; Grimme, C. J.; Dalal, R. J.; Hanson, M. G.; Hexum, J. K.; Reineke, T. M. Polymeric Delivery of Therapeutic Nucleic Acids. *Chem. Rev.* **2021**, *121*, 11527–11652.
- (15) Lächelt, U.; Wagner, E. Nucleic Acid Therapeutics Using Polyplexes: A Journey of 50 Years (and Beyond). *Chem. Rev.* **2015**, *115*, 11043–11078.
- (16) Yin, H.; Kanasty, R. L.; Eltoukhy, A. A.; Vegas, A. J.; Dorkin, J. R.; Anderson, D. G. Non-Viral Vectors for Gene-Based Therapy. *Nat. Rev. Genet.* **2014**, *15*, 541–555.
- (17) Kumar, R.; Le, N.; Oviedo, F.; Brown, M. E.; Reineke, T. M. Combinatorial Polycation Synthesis and Causal Machine Learning Reveal Divergent Polymer Design Rules for Effective PDNA and Ribonucleoprotein Delivery. *JACS Au* **2022**, *2*, 428–442.
- (18) Mintzer, M. A.; Simanek, E. E. Nonviral Vectors for Gene Delivery. *Chem. Rev.* **2009**, *109*, 259–302.
- (19) Donahue, N. D.; Acar, H.; Wilhelm, S. Concepts of Nanoparticle Cellular Uptake, Intracellular Trafficking, and Kinetics in Nanomedicine. *Adv. Drug Deliv. Rev.* **2019**, *143*, 68–96.
- (20) Luthman, H.; Magnusson, G. High Efficiency Polyoma DNA Transfection of Chloroquine Treated Cells. *Nucleic Acids Res.* **1983**, *11*, 1295–1308.
- (21) Cheng, J.; Zeidan, R.; Mishra, S.; Liu, A.; Pun, S. H.; Kulkarni, R. P.; Jensen, G. S.; Bellocq, N. C.; Davis, M. E. Structure–Function Correlation of Chloroquine and Analogues as Transgene Expression Enhancers in Nonviral Gene Delivery. *J. Med. Chem.* **2006**, *49*, 6522–6531.
- (22) Zhang, B.; Zhang, Y.; Mallapragada, S. K.; Clapp, A. R. Sensing Polymer/DNA Polyplex Dissociation Using Quantum Dot Fluorophores. *ACS Nano* **2011**, *5*, 129–138.
- (23) Xie, Y.; Yu, F.; Tang, W.; Alade, B. O.; Peng, Z. H.; Wang, Y.; Li, J.; Oupický, D. Synthesis and Evaluation of Chloroquine-Containing DMAEMA Copolymers as Efficient Anti-MiRNA Delivery Vectors with Improved Endosomal Escape and Antimigratory Activity in Cancer Cells. *Macromol. Biosci.* **2018**, *18*, 1700194–1700210.
- (24) Boratyński, P. J.; Zielińska-Blajet, M.; Skarzewski, J. Cinchona Alkaloids—Derivatives and Applications. *Alkaloids-Chem. Biol.* **2019**, *82*, 29–145.
- (25) Achan, J.; Talisuna, A. O.; Erhart, A.; Yeka, A.; Tibenderana, J. K.; Baliraine, F. N.; Rosenthal, P. J.; D’Alessandro, U. Quinine, an Old Anti-Malarial Drug in a Modern World: Role in the Treatment of Malaria. *Malar. J.* **2011**, *10*, 144.
- (26) Luis, F.; Moncayo, G. *Cinchona Alkaloids in Synthesis and Catalysis*, 1st ed.; Song, C. E., Ed.; Wiley: KGaA, Weinheim, 2009.
- (27) Punihaole, D.; Workman, R. J.; Upadhyay, S.; Van Bruggen, C.; Schmitz, A. J.; Reineke, T. M.; Frontiera, R. R. New Insights into Quinine–DNA Binding Using Raman Spectroscopy and Molecular Dynamics Simulations. *J. Phys. Chem. B* **2018**, *122*, 9840–9851.
- (28) Lai, X.; Lin, Y.; Zhang, C.; Zhou, X. Study on the Interaction between Quinine Sulfate and DNA by Multiple Spectral Methods and Their Analytical Applications. *Anal. Sci.* **2013**, *29*, 435–440.
- (29) Parvez, M. M.; Haraguchi, N.; Itsuno, S. Synthesis of Cinchona Alkaloid-Derived Chiral Polymers by Mizoroki-Heck Polymerization and Their Application to Asymmetric Catalysis. *Macromolecules* **2014**, *47*, 1922–1928.
- (30) Kobayashi, N.; Iwai, K. Functional Polymers. 1. Poly(Cinchona Alkaloid-Co-Acrylonitrile)s. New Polymer Catalysts for Asymmetric Synthesis. *J. Am. Chem. Soc.* **1978**, *100*, 7071–7072.

- (31) Van Bruggen, C.; Punihaole, D.; Keith, A. R.; Schmitz, A. J.; Tolar, J.; Frontiera, R. R.; Reineke, T. M. Quinine Copolymer Reporters Promote Efficient Intracellular DNA Delivery and Illuminate a Protein-Induced Unpacking Mechanism. *Proc. Natl. Acad. Sci. U.S.A.* **2020**, *117*, 32919–32928.
- (32) Odian, G. *Principles of Polymerization*; John Wiley & Sons, Inc.: Hoboken, NJ, USA, 2004; pp 263–364.
- (33) Ullah, M. S.; Itsuno, S. Synthesis of Cinchona Alkaloid Squaramide Polymers as Bifunctional Chiral Organocatalysts for the Enantioselective Michael Addition of  $\beta$ -Ketoesters to Nitroolefins. *Mol. Catal.* **2017**, *438*, 239–244.
- (34) Edward, J. A.; Kiesewetter, M. K.; Kim, H.; Flanagan, J. C. A.; Hedrick, J. L.; Waymouth, R. M. Organocatalytic Synthesis of Quinine-Functionalized Poly(Carbonate)S. *Biomacromolecules* **2012**, *13*, 2483–2489.
- (35) Inagaki, M.; Hiratake, J.; Yamamoto, Y.; Oda, J. Asymmetric Induction in the Base-Catalyzed Reactions Using Polymer-Supported Quinines with Spacer Groups. *Bull. Chem. Soc. Jpn.* **1987**, *60*, 4121–4126.
- (36) Moon Kim, B.; Sharpless, K. B. Heterogeneous Catalytic Asymmetric Dihydroxylation: Use of a Polymer-Bound Alkaloid. *Tetrahedron Lett.* **1990**, *31*, 3003–3006.
- (37) Onimura, K.; Matsuzaki, K.; Lee, Y. K.; Tsutsumi, H.; Oishi, T. Facile Synthesis of Polymer-Supported Cinchona Alkaloid Catalysts for Asymmetric Michael Reaction. *Polym. J.* **2004**, *36*, 190–197.
- (38) Haynes, W. M. *CRC Handbook of Chemistry and Physics*; CRC Press, 2014.
- (39) Kumar, R.; Le, N.; Tan, Z.; Brown, M. E.; Jiang, S.; Reineke, T. M. Efficient Polymer-Mediated Delivery of Gene-Editing Ribonucleoprotein Payloads through Combinatorial Design, Parallelized Experimentation, and Machine Learning. *ACS Nano* **2020**, *14*, 17626–17639.
- (40) Sprouse, D.; Reineke, T. M. Investigating the Effects of Block versus Statistical Glycopolycations Containing Primary and Tertiary Amines for Plasmid DNA Delivery. *Biomacromolecules* **2014**, *15*, 2616–2628.
- (41) Behr, J.-P. The Proton Sponge: A Trick to Enter Cells the Viruses Did Not Exploit. *Chimia* **1997**, *51*, 34.
- (42) Vermeulen, L. M. P.; De Smedt, S. C.; Remaut, K.; Braeckmans, K. The Proton Sponge Hypothesis: Fable or Fact? *Eur. J. Pharm. Biopharm.* **2018**, *129*, 184–190.
- (43) Bus, T.; Traeger, A.; Schubert, U. S. The Great Escape: How Cationic Polyplexes Overcome the Endosomal Barrier. *J. Mater. Chem. B* **2018**, *6*, 6904–6918.
- (44) Li, Y.; Zhao, T.; Wang, C.; Lin, Z.; Huang, G.; Sumer, B. D.; Gao, J. Molecular Basis of Cooperativity in PH-Triggered Supramolecular Self-Assembly. *Nat. Commun.* **2016**, *7*, 13214.
- (45) Molinspiration Interactive logP Calculator, <https://molinspiration.com/services/logp.html> (accessed May 27, 2021).
- (46) Uccello-Barretta, G.; Bari, L. D.; Salvadori, P. Autoaggregation Phenomena in Quinine Solutions. *Magn. Reson. Chem.* **1992**, *30*, 1054–1063.
- (47) Zhu, M.; Nie, G.; Meng, H.; Xia, T.; Nel, A.; Zhao, Y. Physicochemical Properties Determine Nanomaterial Cellular Uptake, Transport, and Fate. *Acc. Chem. Res.* **2013**, *46*, 622–631.
- (48) Ren, J.; Andrikopoulos, N.; Velonia, K.; Tang, H.; Cai, R.; Ding, F.; Ke, P. C.; Chen, C. Chemical and Biophysical Signatures of the Protein Corona in Nanomedicine. *J. Am. Chem. Soc.* **2022**, *144*, 9184–9205.
- (49) Cam, C.; Segura, T. Matrix-Based Gene Delivery for Tissue Repair. *Curr. Opin. Biotechnol.* **2013**, *24*, 855–863.
- (50) Pannier, A. K.; Shea, L. D. Controlled Release Systems for DNA Delivery. *Mol. Ther.* **2004**, *10*, 19–26.
- (51) Gratton, S. E. A.; Ropp, P. A.; Pohlhaus, P. D.; Luft, J. C.; Madden, V. J.; Napier, M. E.; DeSimone, J. M. The Effect of Particle Design on Cellular Internalization Pathways. *Proc. Natl. Acad. Sci.* **2008**, *105*, 11613–11618.
- (52) Grigsby, C. L.; Leong, K. W. Balancing Protection and Release of DNA: Tools to Address a Bottleneck of Non-Viral Gene Delivery. *J. R. Soc. Interface* **2010**, *7*, S67–S82.
- (53) Won, Y.-Y.; Sharma, R.; Konieczny, S. F. Missing Pieces in Understanding the Intracellular Trafficking of Polycation/DNA Complexes. *J. Controlled Release* **2009**, *139*, 88–93.
- (54) Wattiaux, R.; Laurent, N.; Wattiaux-De Coninck, S.; Jadot, M. Endosomes, Lysosomes: Their Implication in Gene Transfer. *Adv. Drug Deliv. Rev.* **2000**, *41*, 201–208.
- (55) Boyle, W. S.; Senger, K.; Tolar, J.; Reineke, T. M. Heparin Enhances Transfection in Concert with a Trehalose-Based Polycation with Challenging Cell Types. *Biomacromolecules* **2017**, *18*, 56–67.
- (56) Costes, S. V.; Daelemans, D.; Cho, E. H.; Dobbin, Z.; Pavlakis, G.; Lockett, S. Automatic and Quantitative Measurement of Protein-Protein Colocalization in Live Cells. *Biophys. J.* **2004**, *86*, 3993–4003.